Epitaxial SnO_2 thin films grown on $(\bar{1}012)$ sapphire by femtosecond pulsed laser deposition

J. E. Dominguez, X. Q. Pan,[a] and L. Fu
Department of Materials Science and Engineering, University of Michigan, Ann Arbor, Michigan 48109

P. A. Van Rompay, Z. Zhang, J. A. Nees, and P. P. Pronko
Center for Ultrafast Optical Science and Department of Electrical Engineering and Computer Science, University of Michigan, Ann Arbor, Michigan 48109

(Received 17 April 2001; accepted for publication 28 September 2001)

An ultrafast (100 fs) Ti sapphire laser (780 nm) was used for the deposition of SnO_2 thin films. The laser-induced plasma generated from the SnO_2 target was characterized by optical emission spectroscopy and electrostatic energy analysis. It was found that the ionic versus excited-neutral component ratio in the plasma plume depends strongly on the amount of background oxygen introduced to the deposition chamber. Epitaxial SnO_2 films with high quality and a very smooth surface were deposited on the $(\bar{1}012)$ sapphire substrate fabricated at 700 °C with an oxygen background pressure of ~0.1 mTorr. The films are single crystalline with the rutile structure, resulting from the high similarity in oxygen octahedral configurations between the sapphire $(\bar{1}012)$ surface and the SnO_2 (101) surface. Hall effect measurements showed that the electron mobility of the SnO_2 film is lower than that of bulk single crystal SnO_2, which is caused by the scattering of conduction electrons at the film surface, substrate/film interface, and crystal defects. © *2002 American Institute of Physics.* [DOI: 10.1063/1.1426245]

I. INTRODUCTION

Tin dioxide (SnO_2) with the rutile structure is an *n*-type semiconductor with a wide band gap (3.6 eV). Due to its electrical, optical, and electrochemical properties, SnO_2 is widely used as transparent electrodes in solar cells, flat panel displays, and chemical sensors. Recently, SnO_2 has been integrated into micromachined silicon devices as a sensing element of microsensors.[1,2] SnO_2 thin films have been fabricated using different techniques including electron beam evaporation,[3] rf sputtering,[4,5] and chemical vapor deposition.[6,7] One of the major challenges in synthesizing SnO_2 thin films is the control over stoichiometry. Since most depositions are carried out in high vacuum condition at high temperatures, the SnO_2 films obtained are nonstoichiometric and frequently consist of metastable phases such as SnO and Sn_3O_4.[3,8,9] The existence of these metastable phases and crystal defects will strongly affect the properties of the films.[10,11] Therefore, a postdeposition annealing in air is necessary to obtain the stoichiometric SnO_2 phase with the rutile structure. However, the microstructure of the resulting SnO_2 films is mainly controlled by the annealing process and a number of crystal defects are frequently observed in these films.[11,12]

Pulsed laser deposition (PLD) has proved to be a promising method for producing complex inorganic thin films, such as the films of high T_c superconductors and perovskite oxides. In comparison with other methods, PLD has the capability of controlling many process parameters, such as laser pulse width, energy, and wavelength along with background reactive gas pressure and substrate bias and temperature. Adjusting these parameters provides tunability to the laser plasma thereby allowing for optimum process conditions in a particular thin film deposition.[13] The deposition of oxide thin films using PLD can occur in a reactive atmosphere with adjustable oxygen pressure, which allows the formation of stoichiometric oxides. SnO_2 films and nanopowders synthesized using PLD with a nanosecond pulsed laser have been reported.[14–16] In this article, a femtosecond (fs) pulsed laser is used to synthesize SnO_2 thin films.

Our interest in using femtosecond pulsed laser deposition (fPLD) for this work stems from the fact that there is a significant difference associated with the laser pulse interaction in the target compared to that of the nanosecond case. This difference is found in the brevity and intensity of the femtosecond ablation pulse. Such pulses have minimal or no thermal diffusion associated with them during the initial energy deposition. High ionization states are achieved initially and these ions expand in an ambipolar plasma field together with normal hydrodynamic expansion.[17,18] The equilibrium conditions of the plasma are found to be different from those formed by nanosecond pulses where thermal plasma heating is dominant.[19] For example, these differences consist of plasma electron temperatures being lower for femtosecond pulses along with there being a component of high energy ions in the ablation plume. The formation of very thin plasmas, which are not optically pumped by the incoming laser beam, as is the case for nanosecond pulses, provides a method for eliminating particulate contamination in deposited films.[20] The properties of femtosecond laser plasmas continue to be studied by us, and others,[21] and the signifi-

[a]Author to whom correspondence should be addressed; electronic mail: panx@umich.edu

cance of these properties is still under investigation concerning their use in thin film deposition. The present report is part of that ongoing study and demonstrates that epitaxial SnO_2 thin films with single crystal quality can be fabricated on $(\bar{1}012)$ sapphire substrates at 700 °C using femtosecond pulsed laser deposition.

II. EXPERIMENT

A femtosecond Ti sapphire laser with repetition rate of 10 Hz was used to deposit SnO_2 films. The wavelength of the laser was centered at 780 nm and the pulse width was nominally 100 fs. The target was made by pressing a pure SnO_2 powder (99.99%) followed by sintering at 1100 °C. The base pressure in the deposition chamber was 10^{-9} Torr and the oxygen backfill pressure, during plume analysis, was controlled at 8×10^{-4} Torr using a precision leak valve. The laser-induced plasma plume of SnO_2 was analyzed using an electrostatic energy analyzer, in which ions pass between two spherical-sector plates, and by a time-resolved optical emission spectroscopy. Variable voltage up to 5000 V was applied on each of the plates. Optical emission during plasma relaxation was studied by imaging the laser-induced plasma to an optical fiber attached to a wavelength depressive spectrometer. Time-resolved optical-emission spectra were taken by varying the data collection time delay with respect to the laser pulse. This method provides a way to study the expanding laser-induced plasma on a time scale from nanoseconds to microseconds.

The SnO_2 thin films were deposited at different temperatures on single crystal α-Al_2O_3 (sapphire) having a $(\bar{1}012)$ (*R*-cut) surface orientation. A backfill, with discharge-activated oxygen, was used during deposition. After deposition, the film was naturally cooled under the same vacuum condition as for the deposition process.

The microstructure and morphology of deposited films were characterized using x-ray diffraction (XRD), transmission electron microscopy (TEM), and atomic force microscopy (AFM). For the x-ray diffraction studies, both θ–2θ scans and pole figures were carried out on a rotating anode four-circle diffractometer (Rigaku, Japan) using Cu $K\alpha$ radiation. AFM studies were performed on a Nanoscope III atomic force microscope (Digital Instruments, Inc., CA). Both plan-view and cross-section TEM specimens were prepared by a standard procedure, which includes mechanical grinding, polishing, precision dimpling, and ion milling. The final thinning of specimens was carried out on a Gatan precision ion polishing system (PIPS™, Model 691) using an accelerating voltage of 4 kV and an incident angle of 4°. All specimens were investigated in a JEOL JEM 4000EX high-resolution electron microscope, operated at 400 kV, providing a point resolution of 0.17 nm.

Electrical measurements were performed using a four-point van der Pauw contact arrangement. Hall measurements were performed inside a gas reactor, using a magnetic field of about 2.2 kG. The measurements were performed in a temperature range from room temperature to 625 K, in nitrogen to avoid interference from chemisorbed or diffused oxygen.

III. RESULTS

Plots in Fig. 1(a) are time-resolved optical emission spectra showing the time evolution of the plasma relaxation. Each trace was delayed by a 15 ns interval. The peaks include six excited neutral Sn emission lines. The signal with no delay shows a relatively high value of background and peak broadening compared to longer delay times. As the delay time is increased, both the background emission intensity and the width of the emission line decrease. Under local thermodynamic equilibrium conditions, the plasma temperature can be extracted from the ratio of emission line-to-continuum intensity, indicating plasma temperature decay with position from the target. Figures 1(b) and 1(c) show the ion energy spectra of SnO_2 plumes in vacuum and with 0.8 mTorr discharge-activated oxygen atmosphere, respectively. Seen in the figures are the distributions of observable ionized species as a function of energy. For similar ion energies, there is a decrease of about one order of magnitude in the overall ion density with the introduction of oxygen during ablation.

Using the plasma plume induced by the same femtosecond pulsed laser, SnO_2 thin films were deposited on the $(\bar{1}012)$ sapphire substrate at different temperatures and with various oxygen pressures. Epitaxial films with high crystalline quality were obtained by deposition at 700 °C and with the oxygen pressure of 0.1 mTorr. Figure 2(a) shows a θ–2θ x-ray diffraction pattern of such an epitaxial SnO_2 film. As seen in the figure, in addition to the $\bar{1}012$ and $\bar{2}024$ reflections of the sapphire substrate, the only peak observed for the film is the 101 reflection of the rutile SnO_2 ($2\theta=33.9°$). Figure 2(b) shows the {110} pole-figure of the same SnO_2 film. Only two {110} poles, about 70° away from the center and 100° away from each other, appear in the figure. These two poles are located at the same position of {110} poles in the standard (101) projection of SnO_2. Without changing the orientation of the sample, a $\{11\bar{2}3\}$ pole figure of sapphire substrate was taken (not shown here). By comparing this substrate pole figure with the {110} pole figure of the film, it is found that the SnO_2 film has single crystal quality and grows epitaxially on the $(\bar{1}012)$ sapphire with the in-plane orientation relationship of $SnO_2\,(101)\,[010]\|Al_2O_3\,(\bar{1}012)\,[1\bar{2}10]$.

Figure 3(a) shows an AFM image of the same SnO_2 film as for x-ray diffraction studies. It is seen that the film consists of a smooth surface with a rms roughness of 0.7 nm. Figure 3(b) is a low magnification dark-field image taken in the SnO_2 [010] direction from the same film, showing the film thickness of 100 nm. Planar defects, parallel to each other and lying in the (101) planes are observed. The length and spacing between the defects vary through the image. These planar defects are determined to be antiphase boundaries (APBs) with a lattice displacement of $\frac{1}{2}[\bar{1}01]$. The atomic structure of film/substrate interfaces and crystal defects in the film was studied using high-resolution TEM (HRTEM). Figure 3(c) is a cross-section HRTEM image showing the interfacial structure of a 100-nm-thick film deposited on a $(\bar{1}012)$ sapphire substrate. The electron beam

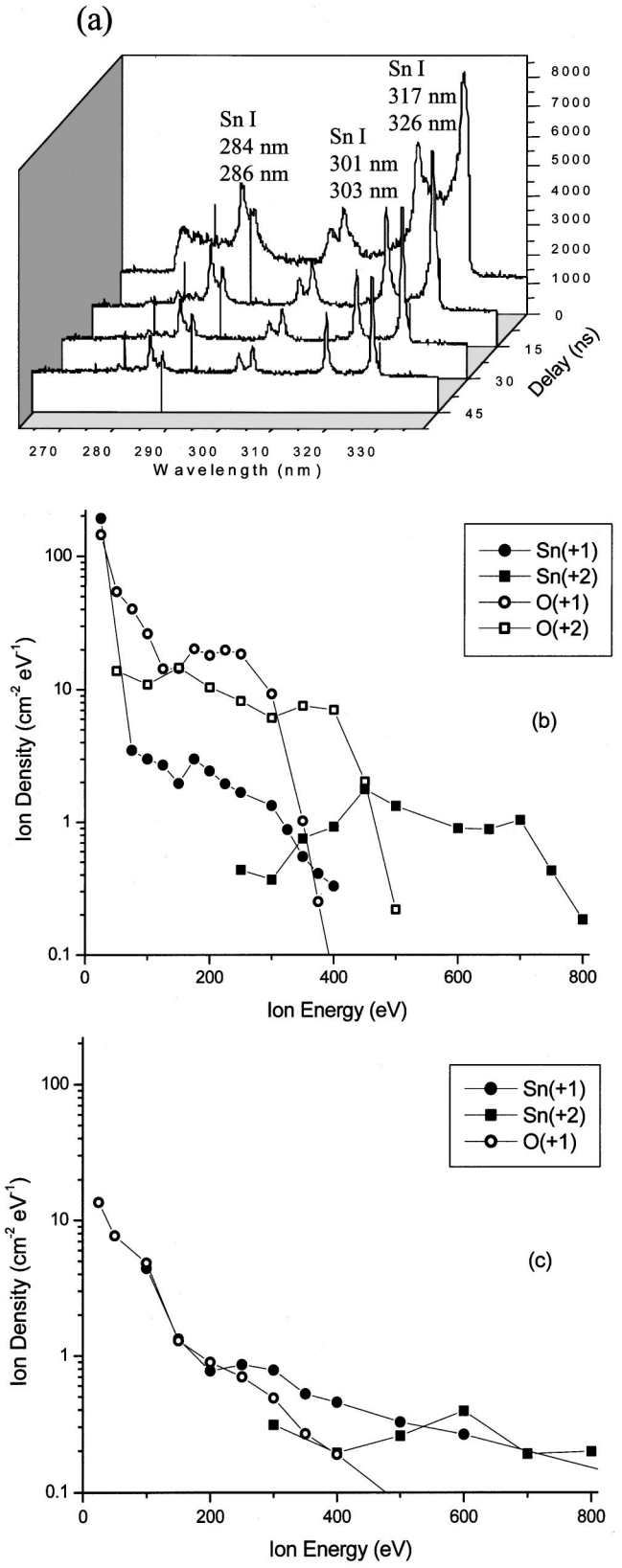

FIG. 1. (a) Optical emission spectra of Sn in the plume at different delay times. (b) Ion energy spectra of Sn and O in plume produced in vacuum. (c) Ion energy spectra of Sn and O in plume produced in 0.8 mTorr oxygen.

was aligned parallel to the [010] direction of SnO_2. It is seen that the SnO_2 film was epitaxially grown on the substrate. Quasiperiodic misfit dislocations, with a spacing of about 2.4 nm, and planar defects running along the length of the film

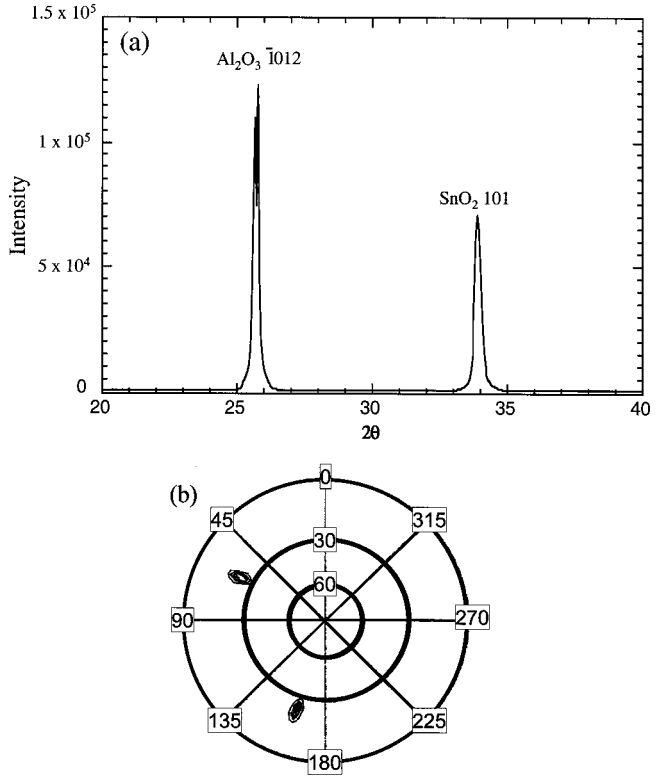

FIG. 2. (a) θ–2θ scan of SnO_2 film grown on $(\bar{1}012)$ sapphire substrate. (b) {110} pole figure of the SnO_2 film.

with a $\frac{1}{2}[\bar{1}01]$ displacement and observed. Figure 3(d) shows an HRTEM image of the interface viewed parallel to the $[\bar{1}01]$ SnO_2 direction. In this direction, there are no misfit dislocations present at the interface and the SnO_2/Al_2O_3 interface is fully coherent. From Figs. 3(a) and 3(b) the crystallographic orientation relationship between the film and the substrate is $SnO_2(101)[010]\|Al_2O_3(\bar{1}012)[1\bar{2}10]$, which confirms the results from x-ray diffraction.

Hall effect measurements showed that the epitaxial SnO_2 films studied in this work was an *n*-type semiconductor with relatively high conductivity value. Figure 4(a) shows the electrical conductivity and the electron concentration of the single crystal film with a thickness of 100 nm, as a function of inverse absolute temperature. From Fig. 4(a), the calculated activation energy of the free electrons is 0.07 eV. The electron concentration and conductivity of the film are relatively high ($>10^{19}\,cm^{-3}$) which indicates that there is a large number of oxygen vacancies in the film. Figure 4(b) shows the corresponding Hall mobility dependence on inverse temperature. The electron concentration increases with increasing temperature, whereas the mobility decreases with increasing temperature, confirming the semiconducting behavior of the material.

IV. DISCUSSION

Qualitatively speaking, the plasma temperature decay with time will be reflected in a decrease of the line to continuum ratio as observed in Fig. 1. The linewidth of the emission signal can be attributed to a Stark broadening mecha-

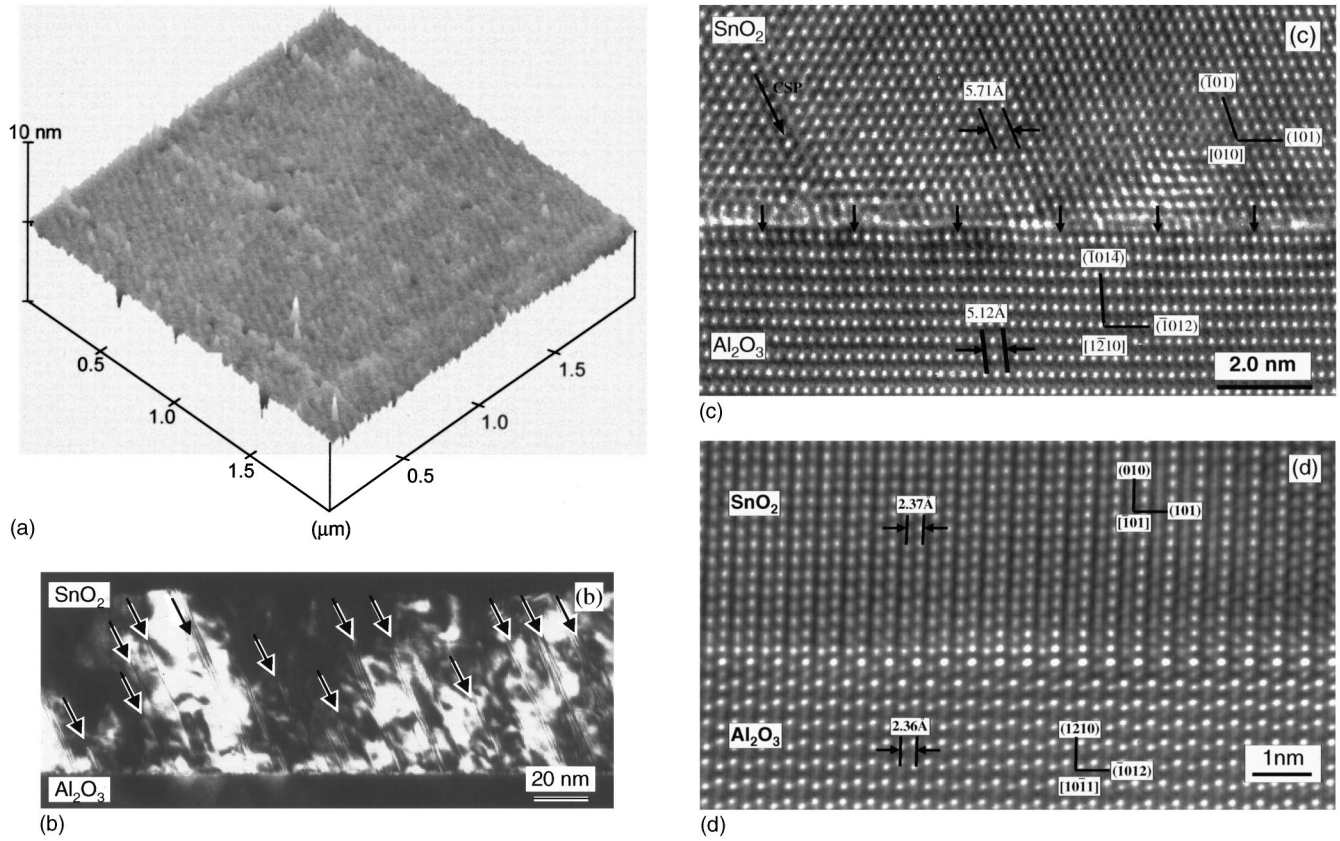

FIG. 3. (a) AFM image of the SnO_2 film on Al_2O_3. (b) Low magnification dark-field image of the film showing planar defects. (c) HRTEM micrograph of the interface between SnO_2 and Al_2O_3 viewed in the SnO_2 [010] direction. (d) HRTEM micrograph of the interface between SnO_2 and Al_2O_3 viewed in the $[\bar{1}01]$ SnO_2 direction.

nism resulting from collisions of charged particles in the plasma. Due to plasma expansion and charge recombination effects, the electron density in the plasma decreases with delay time. As shown in Fig. 1, the early stage of the plasma ($<$30 ns) represents a dramatically changing condition. However, after that time the excitation condition tends to remain relatively constant due to decreased collisions in the plasma. This condition persists until the plasma reaches the deposition substrate. Figures 1(b) and 1(c) show a decrease in ion density with the introduction of oxygen in the deposition chamber. The decrease in both Sn and O ion density, with the introduction of O_2 is related to neutralization charge-exchange interactions of the ions with the controlled volume of gas atoms in the chamber.

These studies show that the plume induced by a femtosecond laser pulse consists of a large number of energetic ions, of which the energy extends to several hundred electron volts. For the deposition of thin films, the existence of such energetic ions can enhance the atomic diffusion at the substrate surface and thus may be useful for the deposition of some materials, which may be difficult to grow under con-

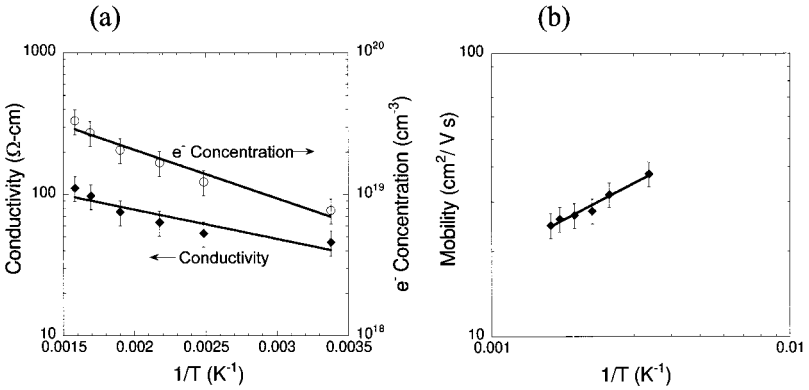

FIG. 4. Electrical properties of the SnO_2 film as a function of inverse temperature. (a) Conductivity and electron concentration, (b) mobility.

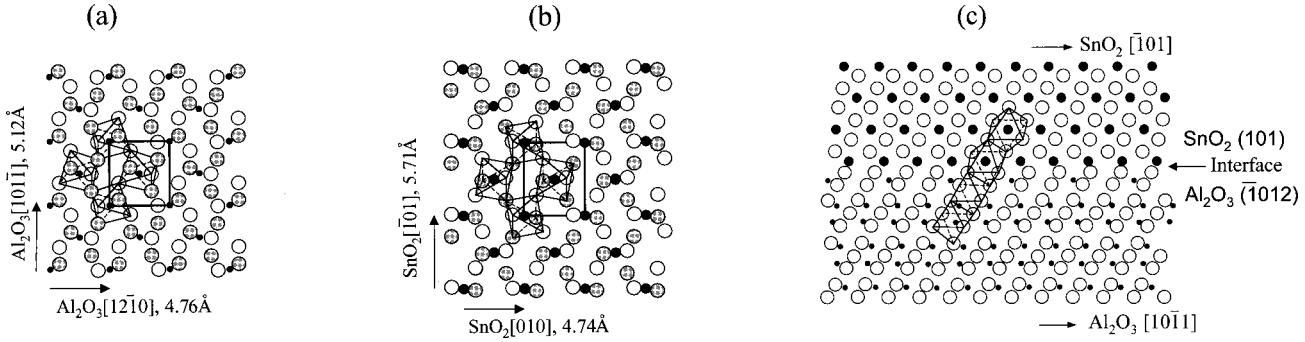

FIG. 5. (a) Surface structure of $(\bar{1}012)$ sapphire. (b) Surface structure of (101) SnO_2. Small filled circles in (a) indicate aluminum atoms and large filled ones in (b) display tin atoms. The large open circles show the oxygen atoms above the plane of metallic atoms, while the shadowed ones represent the oxygen atoms below the metal plane. (c) SnO_2/Al_2O_3 interfacial structure viewed parallel to the SnO_2 [010] direction.

ventional conditions. The enhanced atomic diffusion at the film surface could also reduce the surface roughness. On the other hand, the energetic ions have a sputtering effect at the film surface, which could significantly slow down the growth rate of the film. As shown in Figs. 1(b) and 1(c), the energy of ions in the plume can be reduced by the introduction of oxygen in the growth chamber. Furthermore, the interaction (collision) between the energetic ions and oxygen atoms in the background will increase the kinetic energy of oxygen atoms and enhance the incorporation of oxygen atoms with the film surface, which may enable the deposition of oxide thin films at low oxygen background pressure. Therefore, it is possible to optimize the deposition conditions to obtain oxide thin films with desirable structures and properties. For SnO_2 thin films, the optimal deposition conditions are at 700 °C and with an oxygen background pressure of 0.1 mTorr.

XRD and TEM results show that the SnO_2 film grows epitaxially on the $(\bar{1}012)$ surface of sapphire with the orientation relationship of $SnO_2\,(101)\,[010] \| Al_2O_3\,(\bar{1}012)\,[1\bar{2}10]$. This is consistent with previous results for SnO_2 deposited by sputtering on the same sapphire substrate orientation.[1] The lattice mismatch across the film/substrate interface is 11.45% along the $SnO_2[\bar{1}01]$ direction (which is parallel to the $[10\bar{1}1]$ direction of Al_2O_3) and -0.42% along the perpendicular direction, that is the [010] direction of SnO_2. As a result, no defects are observed when electron beam is aligned along the $SnO_2[\bar{1}01]$ direction, whereas misfit dislocations and planar defects are seen when the film is viewed in the SnO_2 [010] direction, as shown in Figs. 3(b)–3(d). Despite the relatively large lattice mismatch (~11%) in one direction, the SnO_2 film grows epitaxially on the sapphire substrate. This epitaxial growth is determined by the similarity in the surface structure between the film and the substrate. In the rutile SnO_2 structure, oxygen atoms form edge-shared octahedron chains along the (001) direction and Sn atoms fill one half of the octahedra. In the α-Al_2O_3 (sapphire) structure, oxygen atoms form a sublattice, which has a nearly hcp structure. Al atoms occupy two thirds of the interstitial sites of oxygen octahedra. Figures 5(a) and 5(b) show the atomic configurations of the sapphire $(\bar{1}012)$ surface and the SnO_2 (101) surface. Small filled circles represent aluminum atoms in sapphire and large filled ones display tin atoms in the SnO_2 structure. The large open circles represent the oxygen atoms above the lattice plane of metal atoms, while the shadowed ones indicate the oxygen atoms below the plane of metal atoms. The rectangular repeating unit cell on the $(\bar{1}012)$ surface of sapphire [see Fig. 5(a)] has a periodicity of 5.12 Å along the $[10\bar{1}1]$ direction and 4.76 Å along the $[1\bar{2}10]$ direction. A similar repeating unit cell exists on the (101) surface of SnO_2 [see Fig. 5(b)], with a periodicity of 5.71 Å along the $[\bar{1}01]$ direction and 4.74 Å along the [010] direction. The arrangement of oxygen octahedra at the (101) surface of SnO_2 and the sapphire $(\bar{1}012)$ surface are also shown in Figs. 5(a) and 5(b). The epitaxial growth of SnO_2 may begin with the filling of Al sites by Sn along with a small distortion of oxygen octahedra. Figure 5(c) shows the atomic arrangement of the SnO_2/Al_2O_3 interface viewed along the [010] SnO_2 direction. It is seen that the oxygen octahedral network continues with a small distortion across the SnO_2/Al_2O_3 interface, which favors charge balance and low deformation energy at the interface.

Planar defects such as antiphase boundaries, which are also called coherent crystallographic shear planes (CSPs), are frequently observed in SnO_2 films.[22] In the present case, APBs lie on the (101) planes with a displacement vector of $1/2[\bar{1}01]$. The appearance of CSPs is widely regarded in systems such as TiO_2, WO_3, and V_2O_5 to be due to a form of point defect aggregate.[23] As such, CSPs allow nonstoichiometric phases to be present in the material. In the present case, only APBs are observed, for which the lattice displacement vector lies in the defect plane. Therefore, the film stoichiometry will not be changed at these defects. The occurrence of the APBs may be due to the thermal or mismatch strain between the substrate and the film.

Figure 4 shows that the electron concentration in the SnO_2 film is in the order of $10^{19}\,cm^{-3}$, which agrees with the value of bulk single crystal SnO_2.[24] Studies of undoped single crystal bulk SnO_2 showed that the Hall mobility of electrons at room temperature, for an electron concentration of about $10^{19}\,cm^{-3}$, is around 90 $cm^2/V\,s$.[24] In the present work, the mobility at room temperature is about 37 $cm^2/V\,s$. Planar defects, such as CSPs and antiphase boundaries as

well as interfaces, have been shown to act as scattering centers in nonstoichiometric rutile TiO_2,[25] which significantly reduces the conductivity with respect to perfect crystal. The main defects observed in the SnO_2 thin film fabricated by fPLD are antiphase boundaries (coherent CSPs) and misfit dislocation at the interface. It is recognized that scattering of electrons at the film/substrate interface becomes important with decreasing film thickness. Thus, the low mobility of our SnO_2 film in comparison with bulk single crystal is primarily due to the scattering effects of electrons at defects and at the interface. Other factors such as surface scattering are negligible due to the small value of the mean free path with respect to film thickness. Previous studies of high purity single crystal SnO_2, at high temperatures, had shown that polar optical mode scattering is the predominant scattering mode at temperatures higher than 250 K.[26] The power law dependence of the mobility with temperature, shown in Fig. 4(b), is consistent with the model of lattice vibration scattering at high temperatures.[27]

V. CONCLUSION

In conclusion, the plasma plume produced by ablating a ceramic SnO_2 source with a femtosecond pulsed laser was analyzed. It was found that the ion to excited-neutral ratio in the plasma plume strongly depends on the amount of oxygen in the deposition chamber and the delay time after plasma expansion. Using this unique fPLD, epitaxial SnO_2 thin films with single crystalline quality and very smooth surface were grown on the $(\bar{1}012)$ sapphire substrates at 700 °C with an oxygen background pressure of 0.1 mTorr. The smooth surface of the film results from the thin, homogeneous plasma plume induced by an ultrafast laser. Crystal defects including misfit dislocations and antiphase boundaries were observed in the SnO_2 films, resulting from the lattice mismatch cross the film/substrate interface. The electrical conductivity of the film is governed by oxygen vacancies. The electron mobility depends on the scattering of electrons at crystal defects and interfaces of the film.

ACKNOWLEDGMENTS

This work was supported by the National Science Foundation (NSF) through Grant No. NSF/DMR 9875405 (CAREER, XQP) and through the Center for Ultrafast Optical Science under Grant No. STC PHY 8920108.

[1] S. Semancik and R. E. Cavicchi, Acc. Chem. Res. **31**, 279 (1998).
[2] T. Becker, S. Muhlberger, C. Bosch, V. Braunmuhl, G. Muller, T. Ziemann, and K. V. Hetchtenberg, Sens. Actuators B **69**, 108 (2000).
[3] W. I. Cho, H. Jang, and S. R. Lee, Scr. Metall. Mater. **32**, 815 (1995).
[4] M. Di Giulio, G. Micocci, A. Serra, A. Tepore, R. Rella, and P. Siciliano, Sens. Actuators B **24–25**, 465 (1995).
[5] M. C. Horrillo, P. Serrini, J. Santos, and L. Manes, Sens. Actuators B **45**, 193 (1997).
[6] D. Liu, Q. Wang, H. L. M. Chang, and H. Chen, J. Mater. Res. **10**, 1516 (1995).
[7] Y. Liu, W. Zhu, O. K. Tan, and X. Tao, J. Mater. Sci. **7**, 279 (1996).
[8] M. H. Reddy, S. R. Jawalekar, and A. N. Chandrokar, Thin Solid Films **169**, 117 (1989).
[9] M. R. Soares, P. H. Dionisio, I. J. R. Baumvol, and W. H. Schreiner, Thin Solid Films **214**, 6 (1992).
[10] X. Q. Pan and L. Fu, J. Electroceram. (in press).
[11] X. Q. Pan and L. Fu, J. Appl. Phys. **89**, 6048 (2001).
[12] X. Q. Pan, L. Fu, and J. E. Dominguez, J. Appl. Phys. **89**, 6056 (2001).
[13] J. T. Cheung, in *Pulser Laser Deposition of Thin Films*, edited by D. B. Chrisey and G. H. Huber (Wiley Interscience, New York, 1994), pp. 1–22.
[14] Y. Zhao, Z. Feng, and Y. Liang, Sens. Actuators B **56**, 224 (1999).
[15] R. D. Vispute, V. P. Godbloe, S. M. Chaudhari, S. M. Kanetkar, and S. B. Ogale, J. Mater. Res. **3**, 1180 (1988).
[16] G. Williams and G. S. V. Coles, J. Math. Chem. **8**, 1657 (1998).
[17] P. Pronko, P. Van Rompay, and S. Sato, Proc. SPIE **3269**, 46 (1998).
[18] P. A. VanRompay, M. Nantel, and P. P. Pronko, Appl. Surf. Sci. **127–128**, 1023 (1998).
[19] Z. Zhang, P. A. VanRompay, J. A. Nees, C. A. Stewart, X. Q. Pan, L. Fu, and P. P. Pronko, Proc. SPIE **3935**, 86 (2000).
[20] A. V. Rode, B. Luther-Davies, and E. G. Gamaly, J. Appl. Phys. **85**, 4213 (1999); **85**, 4222 (1999).
[21] A. M. Komashko, M. D. Feit, and A. M. Rubenchik, Proc. SPIE **3935**, 97 (2000).
[22] J. G. Zheng, X. Q. Pan, M. Schweizer, U. Weimar, W. Gopel, and M. Ruhle, J. Mater. Sci. **31**, 2317 (1996).
[23] V. E. Henrich and P. A. Cox, *The Surface Science of Metal Oxides* (Cambridge University Press, Cambridge, 1994), pp. 20–22.
[24] J. A. Marley and R. C. Dockerty, Phys. Rev. **40**, 304 (1965).
[25] A. Inoue and E. Iguchi, J. Phys. C **12**, 5157 (1979).
[26] Z. M. Jarzebski and J. P. Marton, J. Electrochem. Soc. **129**, 299C (1976).
[27] L. L. Kazmerski, *Polycrystalline and Amorphous Thin Films and Devices* (Academic, New York, 1980).